Strongly supercritical non-Boussinesq sustained gravity currents: Time-dependent and steady-state approximate solutions

M. Ungarish*
Department of Computer Science, Technion, Haifa 32000, Israel

(Received 9 January 2023; accepted 5 April 2023; published 8 May 2023)

We consider the flow of an inertial supercritical gravity current sustained by a constant source at $x = 0$ and free drainage edge at $x = x_D$. We analyze time-dependent flows provided by an analytical model and shallow-water finite-difference solution and compare them with the predictions of steady-state formulations [Ellison and Turner, J. Fluid Mech. **6**, 423 (1959); Haddad *et al.*, Phys. Rev. Fluids **7**, 084802 (2022)]. Entrainment and drag (expressed as Eu and $c_D u^2$, respectively, where u is velocity), with coefficients modeled as some simple functions of the Richardson number Ri, play a significant role in the first domain of propagation. The solution shows that an internal forward-moving jump appears, separating the supercritical, significantly mixed, domain at the rear and the free nose at $x_N(t)$ that propagates toward x_D, where t is time. The behavior of the subcritical domain between the jump and the nose depends strongly on the entrainment-drag model, as follows: (a) If E and c_D decay to zero for $\mathrm{Ri} > \mathrm{Ri}_{\mathrm{crit}} < 1$, eventually the jump overflows x_D, leaving behind a steady-state domain of supercritical flow. This contradicts the steady-state model of Haddad *et al.* that postulates a stationary internal jump at $x_S < x_D$ with a critical outflow at x_D. (b) If finite values E and c_D prevail for $\mathrm{Ri} > 1$, the internal jump propagates to a position $x_J > x_S$ but does not overflow x_D for a long time. Some oscillations at x_D appear, which may indicate a backward-moving adjustment wave, but this is a long-time process beyond the accuracy of our shallow-water simulation. The reasons for the discrepancy with the steady-state solutions, and the connections with the experiment of Ellison and Turner, are discussed. A noteworthy insight is that the time-dependent stage is important for the understanding and use of the steady-state results. The free edge may admit a supercritical outflow, and hence the application of a critical flow condition may lead to nonphysical results; outflow over a weir may reflect the internal jumps, and this needs a separate investigation.

DOI: 10.1103/PhysRevFluids.8.053801

I. INTRODUCTION

Gravity current (GC) is a generic name for the flow of a layer of fluid of density ρ into an ambient fluid of a different density ρ_a. Typically, the current is produced either by a fixed volume released from a lock or by a sustaining source at the origin $x = 0$. Such flows occur in nature (winds, oceanic currents, volcanic clouds), hazards (fires, collapse of fuel reservoirs), and various applications (discharge of liquids and gases, drainage systems). The improvement of the understanding and modeling of these flows is bound to be beneficial and therefore is under active research (Ref. [1] and references therein).

The typical two-dimensional (2D) GC flow is defined by the longitudinal depth-averaged velocity $u(x, t)$ and interface $h(x, t)$ (thickness measured from the boundary of propagation), where x and

*unga@cs.technion.ac.il

t are the downstream coordinate and time, respectively. The driving force is the reduced gravity g' (defined below); assuming a large Reynolds number, viscous forces are neglected. The GC propagates at the bottom when $\rho > \rho_a$ and at the top when $\rho < \rho_a$. In a Boussinesq (Bq) system (i.e., $\rho/\rho_a \approx 1$) the bottom and top GC are symmetric. The classical analysis of the GC assumes a stable, smooth, impenetrable interface; in this case, entrainment and drag can be neglected for long distances of propagation [2]. The criterion for the stability of the interface is associated with the Richardson number, $\mathrm{Ri} = g'h/u^2$, which expresses the ratio of the buoyancy stabilizing (settling) effect to the shear destabilizing (rotation) effect on a fluid particle. For a sufficiently small Ri the interface becomes unstable, and the classical GC analysis must be extended to effects of entrainment and drag. In view of the large range of practical source conditions, an initial small Ri must be taken into consideration. In other words, the sustained GC starting in the unstable domain (called supercritical) is a realistic situation. Surprisingly, however, the flow with entrainment and drag may attain steady-state patterns.

The background idea has been provided by Ref. [3], which predicts (and confirms by a simple experiment) that a thin layer of buoyant fluid, sustained by a source over (or below) a thick stationary ambient fluid, will rapidly attain a steady state in the downstream direction. The study considers a situation with strong mixing in the domain close to the source (where the global Richardson number Ri is small) and points out that the mixing subsides after some distance $x > x_m$ (where Ri is not small). However, the paper did not provide a solution for the flow field, and the experimental data are presented only in a reduced form concerning the dependency of entrainment on Ri. Moreover, in the experiments the steady state could be maintained only for a few seconds, after which it was disturbed by an unexpected upstream wave.

A recent paper by Haddad, Vaux, Varrall, and Vauquelin [4] (hereinafter referred to as HVVV) reconsiders this steady-state flow, using a model and large-eddy simulations. They focus attention on a constant-influx 2D sustained top GC that propagates along a horizontal boundary, in a very deep ambient, at high Reynolds number. The study emphasizes three points: The current is non-Bq, steady state, and strongly influenced by mixing-entrainment because the Richardson number at the inlet, Ri_i, is very small (the subscript i denotes the conditions at the inlet). HVVV focus on a light (top) current.

Some open questions remain. The GC is essentially a time-dependent phenomenon. Fluid is injected at $x = 0$ into the stationary ambient. At $t = 0$ the injected fluid is a short domain whose nose $x_N(t)$ begins to propagate with a significant speed, and after a certain time period the nose $x_N(t)$ will reach the free edge x_D. The leap of the analysis to a steady-state flow solution over a long x_D is problematic. It is not clear *a priori* that this solution is compatible with the time-dependent formation. The steady-state model of HVVV contains a stationary internal jump. The question "how and when is this created?" is relevant. An inspection reveals that this is not a unique solution of the steady-state problem. HVVV apply at x_D the condition of critical flow ($\mathrm{Ri} = 1$), but a supercritical outflow is also feasible, as shown below. The need for the clarification of these and related gaps of knowledge motivated the present work. Here we attempt a study of the time-dependent process. As in the system of HVVV, the given conditions are the influx (source) conditions (with subscript i) h_i, u_i, ρ_i and the density of the ambient ρ_a, but we consider the propagation of a free nose $x_N(t)$ toward x_D and the development of the flow between the inlet and the nose, until and after x_N reaches x_D.

The flow of a GC sustained by a constant source $q_i = h_i u_i$ has received considerable attention in the literature. Many recent papers are concerned with flows on a slope (e.g., Refs. [5–7]). In this system, g' has a downstream (along the slope) component that increases the velocity u while the height $h \approx q_i/u$ decreases, and hence $\mathrm{Ri} \propto h/u^2 \approx q_i/u^3$ decreases (see Ref. [1], Sec. 11.2.2). Even for nonsmall initial Ri_i (subcritical or critical source), at some distance from the source the interface develops instabilities, and hence entrainment and drag are essential components. For a horizontal GC (as considered in this paper) the scenario is different, because g' is perpendicular to the flow, and no direct acceleration of u is expected. When the source is subcritical (or even slightly supercritical), the subsequent flow may preserve the nonsmall Ri, in which case the classical models (with zero entrainment and drag) are a good approximation for long distances of propagation [2,8,9].

When the source is strongly supercritical [3,4], entrainment and drag are bound to affect the initial propagation; however, in the horizontal GC, Ri increases with x, and a stabilization of the interface must be taken into account.

Both inclined and horizontal GCs sustained by a constant source may develop domains of steady-state flow. The steady-state solution is certainly important in long-time processes, such as transport in an industrial pipe. However, we must keep in mind that the GC is a time-dependent phenomenon. The realization of a steady state must involve some adjustment stage. In some cases, such as a fire, the time-dependent stage may be more relevant to the user than the steady state, and the source may be turned off before the steady state is established [10]. The present paper is concerned with the time-dependent evolution of supercritical GCs toward a possible steady state.

In the following discussion we assume a 2D gravity current over (or under) a horizontal free-slip solid boundary. The density of the ambient fluid is constant, ρ_a. Let ρ, h, and u be the density of the current, the thickness of the current, and the depth-averaged velocity of the current, respectively. The variables are in general functions of x and t. We define the internal reduced gravity

$$g' = |\rho_a/\rho - 1|g \tag{1}$$

and the internal Froude number

$$\mathcal{F} = u/(g'h)^{1/2}, \tag{2}$$

which expresses the ratio of the local speed of the current to that of the internal gravity wave. (This $\mathcal{F}$ must be distinguished from the Fr_N parameter associated with the jump condition at the nose.) In general, g' and $\mathcal{F}$ are functions of x and t. The flows with $\mathcal{F} = 1$, $\mathcal{F} > 1$, and $\mathcal{F} < 1$ are called critical, supercritical, and subcritical, respectively. Let g'_0 denote the value of g' at the inlet $x = 0$.

For further reference we also define

$$g'_i = |\rho_i/\rho_a - 1|g. \tag{3}$$

The difference between g'_0 and g'_i is negligible in Boussinesq (Bq) systems, but in non-Bq cases it must be taken into account. Note that g'_0 and g'_i are constants in a given system, while g' may vary with x and t when ρ of the GC is affected by entrainment.

The structure of the paper is as follows. We start with predictions of simple models for the time-dependent sustained GC: The classical flow without entrainment and drag is considered in Sec. II A, and the hybrid model (HM) extension (with entrainment and drag) is developed and discussed next. In both cases, when the influx in supercritical, quasisteady domains appear, separated by an internal jump that propagates away from the source. The pattern of the flow changes when the nose and then the internal jump arrive at the drainage position x_D. The model with a stationary jump, suggested by HVVV, is discussed in Sec. II B. The predictions of the HM are presented for typical cases, including the influx conditions of the examples of HVVV. In Sec. III we introduce the more rigorous solution (by finite difference) of the shallow-water (SW) set of equations. We show that there is good agreement with the HM. Comparisons with the results with HVVV are performed, and the differences are discussed. Concluding remarks are given in Sec. IV. In the Appendix a brief derivation of the SW equations is presented.

II. ANALYTICAL MODELS

The flow of the sustained GC is amenable to simple modeling with analytical solutions. (Here, "analytical" includes straightforward numerical tools, such as iterative solution of algebraic equations and integration of ordinary differential equations.) We start with these models because they provide useful insights into the process under investigation.

A. Classical patterns for zero entrainment

When entrainment is negligible, $\rho = \rho_i$ in the current, and hence $g' = g'_0$. The classical (standard) SW one-layer theory (see Appendix and Ref. [1]) provides a simple solution to this problem: The

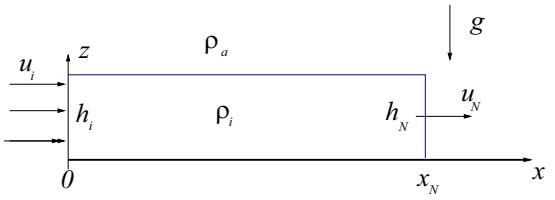

FIG. 1. Classical simple propagating GC with smooth interface.

current has constant height h and propagates with constant speed u_N. We distinguish between two cases.

1. Free propagating current. See Fig. 1. The leading edge of the current is a jump of speed $u_N = \mathrm{Fr}_N(\rho_i/\rho_a)^{1/2}(g_0' h_N)^{1/2}$, where Fr_N is the nose-jump Froude number, $= \sqrt{2}$ according to Benjamin's solution. The value $h = h_N$ is obtained by flux continuity, $q_i = u_i h_i = \mathrm{Fr}_N(\rho_i/\rho_a)^{1/2} g_0'^{1/2} h^{3/2}$. It is convenient to define the buoyancy flux

$$B_0 = |\rho_i/\rho_a - 1| g u_i h_i = g_i' u_i h_i. \tag{4}$$

We can express $u_N = \mathrm{Fr}_N^{2/3} B_0^{1/3}$. This simple solution is quite robust: It is an exact solution of the shallow-water equations for both "top" and "bottom" Bq ($\rho_i/\rho_a \approx 1$) and non-Bq GCs. Moreover, with the exception of the domains close to the inlet and nose, the flow can be considered to be in steady state. The position of the nose is $x_N = u_N t$.

2. Drainage GC. See Fig. 3. An interesting variant of this problem is provided by the presence of a drainage-from-the-edge (or drainage-from-the-free-end) condition at $x = x_D$, where the horizontal solid boundary on which the GC propagates has a sharp end. When the nose x_N reaches this position, the Benjamin-type jump becomes irrelevant and is replaced by an expansion flow. Analysis of the characteristics of the SW equations (see Ref. [11]) shows that u_N must be replaced by the critical flow condition $u_D = |\rho_a/\rho_i - 1| g\sqrt{h_D}$ ($\mathcal{F}_D = 1$). Eventually, a new long (quasisteady-state) GC develops with $u_D h_D = q_i$, and this yields $u_D = ([\rho_a/\rho_i)B_0]^{1/3}$. The adjustment implies a change in volume of the GC in the domain $0 \leqslant x \leqslant x_D$, $\Delta\mathcal{V} = x_D(h_D - h_N)$ (approximately), and the adjustment-time interval is estimated as $|\Delta\mathcal{V}|/q_i$. For Boussinesq and bottom GCs, $u_D < u_N$ [because $\mathrm{Fr}_N(\rho_i/\rho_a)^{1/2} \geqslant \sqrt{2}$] and hence $h_D > h_N$, $\Delta\mathcal{V} > 0$. For top non-Bq GCs, $\mathrm{Fr}_N(\rho_i/\rho_a)^{1/2} < 1$ may occur, leading to $u_D > u_N$ and $h_D < h_N$, $\Delta\mathcal{V} < 0$.

Let us reconsider the inflow side. Ideally, the solution starts at $x = 0$, $t = 0$. However, various considerations indicate that an adjustment interval is expected at the influx boundary. The thin-layer equations are relevant only after some "current" has been developed, i.e., $x_N > h_i$. We shall assume that the adjustment-time and length intervals are negligible on the scale of the system under consideration. A closer inspection of the influx-adjustment region involves the characteristics of the SW equations [8]. Here the important parameter is $\mathcal{F}$. The analysis reveals that the smooth interface of the current, assumed in the classical solution (Fig. 1), is relevant for critical and subcritical influx conditions. For $\mathcal{F}_i > 1$ an internal jump appears (Figs. 2 and 3). We shall focus attention on flows of this type, i.e., with supercritical inflow at the source, when an internal jump appears.

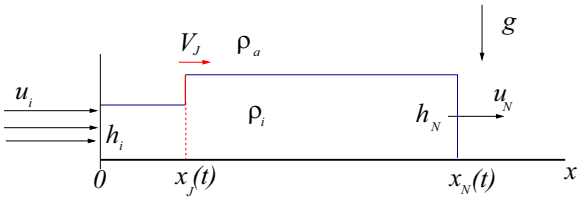

FIG. 2. Classical propagating GC with internal jump.

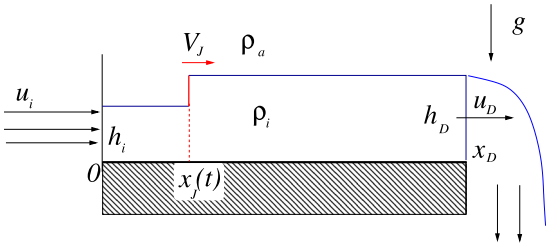

FIG. 3. Drainage GC with internal jump.

B. Models with entrainment

Consider Fig. 4. There is a great deal of evidence (e.g., Refs. [2,3,5]) that the interface between the GC and the ambient fluid becomes unstable for a sufficiently small ratio of buoyancy to shear; this ratio, squared, is referred to as the Richardson number. The precise value of this parameter depends on small-scale details that are unavailable in a depth-averaged simplified flow-field solution. An accepted approximation is the bulk (or overall) Richardson number defined by

$$\mathrm{Ri} = \frac{|\rho_a/\rho - 1|gh}{u^2} = \frac{g'h}{u^2} = \frac{1}{\mathcal{F}^2}. \tag{5}$$

There is evidence that for $\mathrm{Ri} < \mathrm{Ri}_{\mathrm{crit}}$ of the order of 0.3 (i.e., large $\mathcal{F}$) the interface is locally unstable and supports entrainment and mixing of ambient fluid into the moving current. Therefore, when $\mathcal{F}_i \gtrsim 2$, the classical model must be revised. Formally, it is necessary and sufficient to incorporate the contributions of entrainment and drag terms into the simplified equations of motion and seek again quasisteady solutions.

The governing equations (see Appendix) for the steady-state flow in the mixed domain can be expressed as (prime denotes x derivative)

$$\frac{\rho'}{\rho} = -\left(1 - \frac{\rho_a}{\rho}\right)\frac{E}{h}, \tag{6a}$$

$$\frac{u'}{u} = -\frac{1}{(1-\mathrm{Ri})h}\left[E\left(\frac{\rho_a}{\rho} + \frac{1}{2}\mathrm{Ri}\right) + c_D\right], \tag{6b}$$

$$\frac{h'}{h} = \frac{E}{h} - \frac{u'}{u}, \tag{6c}$$

subject to the initial conditions ρ_i, h_i, u_i at $x = 0$ and supplemented by some empirical formulas for E and c_D as functions of $\mathrm{Ri} = \mathrm{Ri}(x) = |1 - \rho_a/\rho|gh/u^2$. As a prototype for the elucidation of our models we take the relationship (see Refs. [1,2])

$$E = 0.075/(1 + 27\mathrm{Ri}); \quad c_D = 0.0065 \quad (\mathrm{Ri} < \mathrm{Ri}_{\mathrm{crit}}), \tag{7}$$

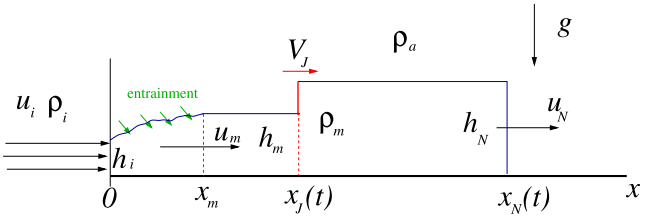

FIG. 4. Mixing steady domain followed by a propagating GC with internal jump.

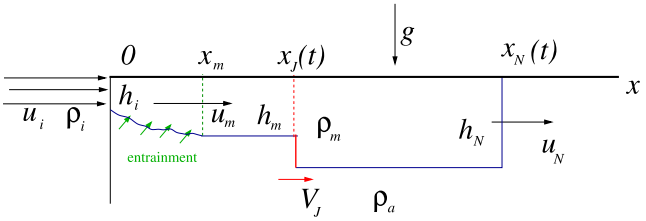

FIG. 5. Sketch of the top GC.

supplemented by $E = c_D = 0$ for $\mathrm{Ri} > \mathrm{Ri}_{\mathrm{crit}}$. (Other relationships will be introduced later.) Equation (7) illustrates the main features of the entrainment and drag: E is $\sim$0.02 for $\mathrm{Ri} \sim 0.1$ and decreases with Ri. c_D is typically smaller than E, but due to more scatter of data it is represented by a constant. The details of the variations of E and c_D have some quantitative influence on the flow-field results. The value of $\mathrm{Ri}_{\mathrm{crit}}$ turns out to have a more dramatic, qualitative effect on the models.

An inspection of (6a)–(6c) indicates a singularity at $\mathrm{Ri} = 1$. The supercritical flow starts with a small $\mathrm{Ri} = \mathrm{Ri}_i$. Then h increases with x due to entrainment, while u decreases due to entrainment and drag; as a result, Ri increases toward the point of singularity. When $\mathrm{Ri}_{\mathrm{crit}} < 1$ the solution of (6a)–(6c) is regular in the process under investigation, while when $\mathrm{Ri}_{\mathrm{crit}} > 1$ the steady-state solution may develop a singularity in the domain of interest. Therefore the cases $\mathrm{Ri}_{\mathrm{crit}} < 1$ and $\mathrm{Ri}_{\mathrm{crit}} > 1$ need different models. (The value of x_D is also significant for the steady-state patterns, but in a rather straightforward manner, and hence the effect of x_D will not be discussed separately.)

1. The hybrid model

We assume that $\mathrm{Ri}_{\mathrm{crit}} < 1$ (for definiteness, we use $\mathrm{Ri}_{\mathrm{crit}} = 0.25$ unless stated otherwise). This implies negligible (zero) entrainment and drag for the domain of subcritical flow where $\mathrm{Ri} > 1$ and $\mathcal{F} < 1$. The appropriate model is called the "hybrid model" (HM) for reasons clarified later.

The reconsideration leads to the following modifications of the classical model.

(1) Following the influx with given ρ_i, h_i, u_i, there is a domain of significant entrainment, $x \leqslant x_m$; see Fig. 4 (the subscript denotes "mixing" or "mixed"). In this domain, ρ_i is mixed (diluted) toward ρ_a, h increases, and u decreases. Consequently, Ri increases monotonically and attains $\mathrm{Ri}_{\mathrm{crit}}$ at x_m. We argue that after a time t_m, the flow in $x \leqslant x_m$ reaches a steady state. The steady-state flow in the mixed domain can be calculated by the integration (e.g., by a Runge-Kutta scheme) of Eqs. (6a)–(6c) (prime denotes x derivative) from $x = 0$ to x_m where $\mathrm{Ri} = \mathrm{Ri}_{\mathrm{crit}}$. The formulation is valid for both bottom and top GCs of Bq and non-Bq type. Like the classical SW formulation used here, the assumption is that the current is a thin layer and the motion of the ambient fluid is negligible. For $0 < \mathrm{Ri} \leqslant \mathrm{Ri}_{\mathrm{crit}} < 1$ (as assumed here) the equations are regular, and the numerical integration is straightforward.

For $x = x_m$ we obtain the steady values ρ_m, h_m, u_m.

(2) Since at x_m the interface becomes stable, the entrainment and drag in the subsequent flow are expected to be insignificant. This implies that for $x > x_m$ the classical SW equations can be applied. The flow will be like that in the classical solution described above (Sec. II A). The only change is in the influx conditions: This flow starts at $x = x_m$ with ρ_m, h_m, u_m; the internal reduced gravity is

$$g'_m = |\rho_a/\rho_m - 1|g. \tag{8}$$

The task is to calculate the flow in $x > x_m$. In general, this is a time-dependent situation. The coincidence between Ri_m and $1/\mathcal{F}_m^2$ is now significant. Since $\mathrm{Ri}_m = \mathrm{Ri}_{\mathrm{crit}} \approx 0.25$, the initial flow at $x = x_m$ is supercritical ($\mathcal{F}_m \approx 2$). Consequently, the flow at $x > x_m$ is expected to contain an internal jump at $x_J(t)$ (Figs. 4 and 5).

The sector $x_m \leqslant x \leqslant x_J(t)$ is expected to be a simple core of constant height and speed h_m, u_m. The speed of the jump is (see Ref. [1], Sec. 4.4)

$$\frac{dx_J}{dt} = V_J = u_m - \mathcal{U}, \tag{9}$$

$$\mathcal{U}^2 = \frac{1}{2} g'_m h^+ (1 + h^+/h_m), \tag{10}$$

where h^+ is the height on the expanded side of the jump. The value of h^+ is determined by the propagation of the current on the expanded side. Here the previous cases are again relevant.

1. Free propagating GC. In this case, the $x > x_J$ domain is approximated as a rectangle of height h_N that propagates with speed $u_N = \mathrm{Fr}_N[(\rho_m/\rho_a) g'_m h_N]^{1/2}$. Evidently, $h^+ = h_N$. We apply the volume-conservation balance to the domain $[x_m, x_N]$: The rate of influx $h_m u_m$ must be accommodated by the displacement of the jumps, i.e., $u_m h_m = h_m V_J + h_N(u_N - V_J)$. Here, h_m and u_m are known, and V_j is given by (9) and (10) (with $h^+ = h_N$). This yields one equation for the unknown h_N. After some algebra we obtain

$$\mathrm{Fr}_N \cdot \left(\frac{\rho_m}{\rho_a}\right)^{1/2} = -\frac{1}{\sqrt{2}} \left(1 + \frac{h_N}{h_m}\right)^{1/2} \left(1 - \frac{h_m}{h_N}\right) + \frac{1}{\sqrt{\mathrm{Ri}_m}} \left(\frac{h_m}{h_N}\right)^{1/2}, \tag{11}$$

where Ri_m is the value of Ri at x_m, taken as $\mathrm{Ri}_{\mathrm{crit}}$.

2. Drainage at x_D. For $x_J(t) \leqslant x \leqslant x_D$ we assume that the GC is a rectangle of height h_D. The corresponding quasisteady state can be calculated by changing the u_N condition above to the critical $u_D = (g'_m h_D)^{1/2}$, and now $h^+ = h_D$. The volume continuity yields the equation for h_D as follows:

$$1 = -\frac{1}{\sqrt{2}} \left(1 + \frac{h_D}{h_m}\right)^{1/2} \left(1 - \frac{h_m}{h_D}\right) + \frac{1}{\sqrt{\mathrm{Ri}_m}} \left(\frac{h_m}{h_D}\right)^{1/2}. \tag{12}$$

Equations (11) and (12) differ only in the left-hand-side term. Since in many typical cases the left-hand side of (11) is quite close to 1, we infer that the free GC and drainage GC display similar flow patterns and can be easily confused by a superficial observation.

The foregoing solution for the GC is called "hybrid model" because we combine a steady-state domain with a time-dependent flow. This type of approximation has been used successfully for axisymmetric GCs in Refs. [12,13]. The major difference here is the presence of entrainment and drag. The solution in the steady-state domain $0 < x \leqslant x_m$ is rigorous [integration of Eqs. (6a)–(6c)], while the time-dependent domain uses the approximation of constant-height interfaces connected by a jump. We do not consider the detailed formation of the domains, and we assume that the internal jump and the front jump appear instantaneously. Evidently, the establishment of the steady-state domain of length x_m requires some time, t_m, which is assumed to be small as compared with the time of observation of the system. (The time t_m can be estimated from the volume of nonambient fluid in $[0, x_m]$, influxed at the rate $u_i h_i$, or by $0.5 x_m/(u_i + u_m)$.) In all the tested cases (see Sec. II C) a significant V_J appears. This indicates that the drainage flow in the domain $x > x_m$ cannot be quasisteady for a long time. The subcritical domain $[x_J, x_D]$ shrinks to zero and is eventually replaced by the faster jet of thickness h_m.

We admit that the entrainment closure (7) lacks rigor. However, the main objective of this investigation is the modeling of the flow, not the quantitative accuracy of the predictions. In this respect, the closure (7) is a fair representation of the available knowledge. For practical use, we keep in mind that the entrainment function and the drag coefficient are adjustable inputs. The value $\mathrm{Ri}_{\mathrm{crit}}$ of transition from unstable to stable interface is also uncertain; however, there are reasons for claiming that the entrainment in a supercritical current (with $\mathrm{Ri}_i \leqslant 0.1$) becomes insignificant after $\mathrm{Ri}(x)$ attains a value of about 0.5. Consider the change in (6a): The factor $(1 - \rho_a/\rho)$ decreases, the factor $1/h$ decreases, and E decreases as $(1 + 27 \times 0.1)/(1 + 27 \times 0.5) = 0.26$. The order of magnitude of the entrainment terms (a normal velocity component) is in the range of uncertainty of the depth-averaged thin-layer approximation. For example, consider the volume

continuity equation for $E = 0.003$ corresponding to $\mathrm{Ri} \approx 0.8$. In this case, the steady-state solution actually assumes that $\partial h/\partial t$ is much smaller than $0.003u$. Therefore a small perturbation of the interface, which can be expected in a realistic GC, invalidates the steady-state balance. We note that Ref. [3] observed that entrainment stops and turbulence subsides at a certain $\mathrm{Ri}_{\mathrm{crit}}$. (They suggest 0.8 but report uncertainties in the measurements of the variables that determine this parameter; more recent and accurate experiments (e.g., Ref. [5]) suggest values around 0.3. We therefore use the theoretically supported value $\mathrm{Ri}_{\mathrm{crit}} = 0.25$ (unless stated otherwise).)

We did some tests with different plausible choices of $\mathrm{Ri}_{\mathrm{crit}}$. The qualitative structure of the flow field is unchanged. We shall return to this issue in Sec. III.

The HM and the SW model discard the viscous forces. The formal justification is that the influx Reynolds number $\mathrm{Re}_i = (h_i u_i/\nu)$ is large, where ν is the kinematic viscosity coefficient of the current. However, as the GC extends, the friction area increases. We therefore use the more relevant effective Reynolds number (Ref. [1], Eq. (3.64))

$$\mathrm{Re}_e \approx (h_i u_i/\nu)(h_i/x_N) = \mathrm{Re}_i(h_i/x_N). \tag{13}$$

The validity of the present inertia-buoyancy models is limited to a propagation x_N/h_i that keeps the value of Re_e sufficiently large (say, 10).

Finally, we note that the foregoing analysis assumes $x_D > x_m$. If $x_D \leqslant x_m$, we integrate (6a)–(6c) numerically from $x = 0$ to x_D. This is the steady-state solution for the entire domain.

2. *Steady-state flow in* $0 \leqslant x \leqslant x_D$*: HVVV model*

The HM shows that when $\mathrm{Ri}_{\mathrm{crit}} < 1$, the time-dependent GC evolves into a steady-state flow over $0 < x < x_D$. This is a smooth solution. h, u, ρ vary with x to h_m, u_m, ρ_m at x_m and then remain constant. The outflow is supercritical, with $\mathrm{Ri}_D = \mathrm{Ri}_{\mathrm{crit}}$. The internal jump at $x_J(t)$ has been spilled out at time t_2 when it has reached x_D.

HVVV argue that a steady state with an internal jump at a fixed $x_S < x_D$ is also feasible. Using $V_J = 0$ combined with (9) and (10) yields

$$r^2 + r - 2/\mathrm{Ri}_S = 0, \tag{14}$$

where $r = h_S^+/h_S$. The positive root [see Eq. (17)] gives acceptable values for plausible upstream $\mathrm{Ri}_S < 1$. However, the downstream Ri_S^+ is always larger than 1. A classical GC (with no entrainment and drag), of constant h_D, cannot match the subcritical flow at x_S^+ with the critical flow at x_D. The conclusion is that a stationary jump cannot appear for $\mathrm{Ri}_{\mathrm{crit}} < 1$.

Indeed, the model of HVVV does not impose the $\mathrm{Ri}_{\mathrm{crit}} < 1$ restriction (formally, in the E and c_D correlations, $\mathrm{Ri}_{\mathrm{crit}} = \infty$). This allows for a steady state with a stationary jump at $x_S < x_D$, with a subcritical $\mathrm{Ri}_S < 1$ (on the upstream side), and $\mathrm{Ri}_D = 1$. We repeat briefly the arguments of HVVV. A manipulation of (6a)–(6c) yields (again, the prime denotes x derivative)

$$\mathrm{Ri}' = \frac{\mathrm{Ri}}{1 - \mathrm{Ri}} \frac{1}{h}[(1 + 2\rho_a/\rho)(1 + \mathrm{Ri}/2)E + 3c_D], \tag{15}$$

and roughly we can approximate (assuming nonlarge values of ρ_a/ρ and Ri)

$$\mathrm{Ri}' \approx \frac{3\mathrm{Ri}}{1 - \mathrm{Ri}} \frac{1}{h}(E + c_D). \tag{16}$$

The sign of Ri' is like that of $(1 - \mathrm{Ri})$. In the initial propagation, Ri increases from the given small Ri_i to some larger $\mathrm{Ri}_S < 1$. Suppose that at x_S there is a stationary jump that yields the downstream $\mathrm{Ri}_S^+ > 1$. The right-hand side of (15) changes sign, and in the domain $x > x_S$ Ri decreases. The condition that the decrease produces $\mathrm{Ri} = 1$ at x_D is expected to determine the value of x_S. This scenario is supported by the following observations.

For the stationary jump, (14) and flux continuity conditions yield

$$\frac{h_S^+}{h_S} = \frac{u_S}{u_S^+} = \frac{1}{2}\beta, \quad \frac{\mathrm{Ri}_S^+}{\mathrm{Ri}_S} = \left(\frac{1}{2}\beta\right)^3, \tag{17}$$

where $\beta = [(1 + 8/\mathrm{Ri}_S)^{1/2} - 1]$. Substitution into (17) shows that for a subcritical $\mathrm{Ri}_S < 1$ we obtain a jump to the supercritical $\mathrm{Ri}_S^+ > 1$. Moreover, for a small Ri_S the leading term is $\mathrm{Ri}_S^+ \approx (8/\mathrm{Ri}_S)^{1/2}$. Next, we note that for $\mathrm{Ri} > 1$, $(E + c_D) \sim 10^{-2}$. For $x > x_S$ the right-hand side of (16) is small, and therefore the decay from Ri_S^+ to 1 will need a significant distance (compared with h_S^+). This confirms the relevance of this scenario to realistic long x_D.

To summarize, the HVVV model uses Eqs. (6a)–(6c) and the same boundary conditions at $x = 0$ as the HM. The supercritical equations are integrated to the position x_S, where a jump occurs. For the jump the HVVV model also uses (9) and imposes $V_J = 0$ by (14), as done here. The major difference is that HVVV do not impose the restriction of entrainment and drag to $\mathrm{Ri} < \mathrm{Ri}_{\mathrm{crit}} < 1$. They argue that the empirical correlations [such as (7)] for E and c_D apply also for nonsmall Ri, including subcritical domains with $\mathrm{Ri} > 1$. In this case the flow after the stationary jump is not constrained to a constant height $h_S = h_D$. Using (17), the steady-state equations (6a)–(6c) are integrated from x_S^+ to the tentative position x_T where $\mathrm{Ri} = 1$ (practically, slightly larger). Imposing $x_T = x_D$, the position x_S is obtained by iterations. Although mathematically correct, we think that this solution lacks convincing physical justification.

The first objection is that it is not clear by which process, and in how much time, this steady state is attained. Second, the need of using the entrainment and drag correlations for large Ri may be a mathematical artifact rather than a physical effect. As explained above, there are good reasons for dismissing the entrainment terms in subcritical flow domains. Furthermore, there is no reason for not accepting the forward propagation of the internal jump during the initial flow of the GC. Therefore the existence of a steady-state flow with a stationary jump at a relatively short distance from the source depends on the existence of a mechanism that arrests, and pushes back, the moving jump. HVVV did not discuss such a mechanism. Finally, the stationary-jump steady-state scenario seems incompatible with the experimental observation of Ref. [3] that the steady state is actually of short duration.

C. Examples of HM results

We illustrate the prediction of the HM model for several cases. The presentation uses both dimensional and dimensionless variables, as specified in the captions of the tables of results. Several plausible scalings are available. In our investigation, the most convenient scaling (suggested by the SW formulation of the next section) uses h_i for length, $U = (g_i' h_i)^{1/2}$ for speed, and h_i/U for time.

1. Top GC

Here we illustrate the predictions of the HM for top GCs; see Fig. 5. To be specific, our examples correspond to the system of two light gases, with the same input properties and geometry as considered by HVVV. In all the examples the density of the ambient is $\rho_a = 1.2\ \mathrm{kg/m^3}$, and $x_D \approx 8$ m. The combinations of the other input parameters are labeled as cases 1–4 and correspond to the same "cases" in the paper of HVVV. The GCs represented by these cases differ in u_i, h_i, ρ_i (dimensional) and thus cover the range $\mathrm{Ri}_i \in [0.003, 0.11]$ (i.e., $\mathcal{F}_i \in [3, 18]$, strongly supercritical) and $\rho_a/\rho_i \in [1.2, 1.6]$ (non-Bq). (The values of Re_i in the simulations of HVVV for these cases were larger than 2×10^4, and hence the viscous effect is negligible in the propagation $x_N/h_i < 100$ considered here.)

The results of the HM for these GCs (cases) are presented in Tables I–III. The three tables cover the same examples (cases 1–4) in different forms: dimensional, scaled using h_i, $(g_i' h_i)^{1/2}$ for lengths and speed, and scaled using h_i, u_i.

TABLE I. Examples for top GC and HM results. Variables are in mks units; $\rho_a = 1.2$. $\mathrm{Ri}_{\mathrm{crit}} = 0.25$.

Case	u_i	h_i	ρ_i	Ri_i	x_m	ρ_m	u_m	h_m	Free-nose V_J	u_N	h_N	Drainage V_J	u_D	h_D
1	8.00	0.10	1.00	0.003	20.63	1.13	1.77	1.32	0.62	1.44	1.85	0.39	1.17	2.32
2	4.20	0.20	0.60	0.111	1.86	0.66	3.11	0.30	0.74	2.13	0.51	0.69	2.06	0.53
3	5.00	0.50	0.75	0.118	4.87	0.79	3.81	0.73	1.06	2.78	1.17	0.84	2.53	1.28
4	10.00	0.50	0.75	0.029	19.12	0.89	4.61	1.59	1.39	3.49	2.44	1.01	3.07	2.79

Note that V_J appears twice in the tables, first for the stage of propagation with a free nose and then for the stage of drainage.

For the tested top GCs the HM works well and predicts physically acceptable flow patterns in accord with Fig. 5. The length x_m and height h_m of the mixed region increase when Ri_i decreases (the flow is more supercritical). The change in density in the mixing domain is reflected by $\Gamma = (\rho_m - \rho_i)/(\rho_a - \rho_i)$. For $\mathrm{Ri}_i \approx 0.1$ the values of Γ are quite small, 0.1. In the extreme supercritical case, case 1, with a very small $\mathrm{Ri}_i = 0.003$, the mixing region is long and thick ($x_m = 206$, $h_m = 13$ scaled with h_i) but $\Gamma = 0.66$ only. In all cases, the internal jump propagates with a significant speed V_J, and this contradicts the expectation that a steady-state pattern with a stationary jump at $x_S < x_m$ appears during the adjustment stages covered by the HM.

We also scaled the speeds with $U_B = B_0^{1/3}$ based on the influx buoyancy flux. The interesting conclusion is that in all tested cases, $u_N/U_B \approx 1.3$ and $u_D/U_B \approx 1.2$, while the internal jump propagates with $V_J/U_B \approx 0.4$.

2. Bottom GC

The top GCs considered above are concerned with gases and may be difficult for laboratory experimental validation. Some more convenient systems are the bottom GCs of saltwater in freshwater, illustrated next. See Fig. 4.

We give examples of four systems (cases), specified in mks units; see Table IV. The cases are labeled as cases 10–13. In all cases, $\rho_i = 1050$ and $\rho_a = 1000$ (water). (For definiteness, let $x_D = 2$ m.) In cases 10–12, $h_i = 0.01$ and $u_i = 1.0, 0.5, 0.2$, and we obtain $\mathrm{Ri}_i = 0.0048$–0.12 (i.e., $\mathcal{F}_i \in [2.9, 14]$). In case 13, $h_i = 0.02$, $u_i = 0.5$, and $\mathrm{Ri}_i = 0.039$ ($\mathcal{F}_i = 5.2$).

The HM yields the results listed in Table IV (dimensional) and Table V (scaled as specified in the caption).

The HM predictions are physically acceptable. The qualitative behaviors of the top and bottom GCs are similar. Again, the internal jump displays a significant speed V_J, and there is no indication of a fixed jump scenario.

III. SW MODEL

The shallow-water (SW) equations express the balances of volume, momentum, and mass of the influxed component, taking into account the entrainment over the interface. A full time-dependent

TABLE II. Examples for top GC and HM results for the same systems (cases) as in Table I, in dimensionless form. Lengths are scaled with h_i, and speed is scaled with $U = \sqrt{g_i' h_i}$ (given in the last column in m/s). $\Gamma = (\rho_m - \rho_i)/(\rho_a - \rho_i)$.

Case	u_i	$\frac{\rho_a}{\rho_i}$	Ri_i	x_m	$\frac{\rho_m}{\rho_i}$	u_m	h_m	Free-nose V_J	u_N	h_N	Drainage V_J	u_D	h_D	Γ	U
1	19.8	1.20	0.003	206	1.13	4.38	13.2	1.54	3.56	18.5	0.97	2.90	23.16	0.66	0.40
2	4.24	2.00	0.111	9.3	1.10	3.14	1.49	0.75	2.15	2.55	0.69	2.08	2.63	0.10	0.99
3	3.69	1.60	0.118	9.7	1.06	2.81	1.46	0.78	2.05	2.33	0.62	1.87	2.56	0.10	1.36
4	7.37	1.60	0.029	38.2	1.19	3.40	3.18	1.02	2.58	4.87	0.75	2.26	5.58	0.32	1.36

TABLE III. Examples for top GC and HM results for the same systems (cases) as in Table I, in dimensionless form. Lengths are scaled with h_i, and speed is scaled with u_i. $\Gamma = (\rho_m - \rho_i)/(\rho_a - \rho_i)$.

Case	$\frac{\rho_a}{\rho_i}$	Ri_i	x_m	$\frac{\rho_m}{\rho_i}$	u_m	h_m	Free-nose V_J	u_N	h_N	Drainage V_J	u_D	h_D	Γ
1	1.2	0.003	206	1.13	0.22	13.2	0.08	0.18	18.46	0.05	0.15	23.16	0.66
2	2.0	0.111	9	1.10	0.74	1.5	0.18	0.51	2.55	0.16	0.49	2.63	0.10
3	1.6	0.118	10	1.06	0.76	1.5	0.21	0.56	2.33	0.17	0.51	2.56	0.10
4	1.6	0.029	38	1.19	0.46	3.2	0.14	0.35	4.87	0.10	0.31	5.58	0.32

process is considered. The equations, in dimensional form, are presented in the Appendix. Here we use dimensionless variables, scaling as follows: length with h_i, velocity with $U = \sqrt{g_i' h_i}$, and time with h_i/U. For the density we use

$$\rho/\rho_a = 1 + s\alpha, \quad s = \rho_i/\rho_a - 1. \tag{18}$$

s is a given constant, positive for the bottom GC and negative for the top GC; $|s| < 1$ in general and $|s| \ll 1$ in a Bq system. Note that $g_i' = |s|g$.

Let $q = uh$ and $\varphi = \alpha h$. We assume $q \geqslant 0$ (confirmed by inspection of the results). The SW dimensionless system for h, q, φ is

$$\frac{\partial h}{\partial t} + \frac{\partial q}{\partial x} = E\frac{q}{h}, \tag{19a}$$

$$\frac{\partial q}{\partial t} + \frac{\partial (q^2/h)}{\partial x} + \frac{1}{2}\frac{1}{(1+s\varphi/h)}\frac{\partial(\varphi h)}{\partial x} = -(q/h)^2\left[c_D - \frac{s\varphi/h}{1+s\varphi/h}E\right], \tag{19b}$$

$$\frac{\partial \varphi}{\partial t} + \frac{\partial(\varphi q/h)}{\partial x} = 0. \tag{19c}$$

The boundary conditions are as follows: At $x = 0$, $h = 1, \varphi = 1$, and $u = u_i$ is given. During propagation, at $x = x_N < x_D$, we use Benjamin's jump condition

$$u_N = dx_N/dt = \mathrm{Fr}_N\sqrt{\varphi} \tag{20}$$

with $\mathrm{Fr}_N = \sqrt{2}$. (After x_N attains x_D, we can change to the critical edge condition $u = [h/(1 + s\varphi/h)]^{1/2}$ at the fixed x_D.)

For initial conditions at $t = 0$, we postulate $h = 1, u = u_i$ for $0 < x < 1$, and $x_N = 1$. Theoretically, the flow starts with a zero GC, but this is inconsistent with the SW equations developed for an existing current. Our start at $t = 0$ is after some plausible quick adjustment. The uncertainty of the initial adjustment region is unimportant because the focus of our solution is long GC ($x_N > 10$).

The system is closed by a correlation for E and c_D as functions of Ri. Substituting the scaling, (18), and definitions of q, φ into (5), the changing $\mathrm{Ri}(x, t)$ is expressed as

$$\mathrm{Ri} = \frac{\varphi h^2}{(1+s\varphi/h)q^2}. \tag{21}$$

TABLE IV. Examples for bottom GC and HM results. Variables are in mks units; $\rho_a = 1000$, $\mathrm{Ri}_{\mathrm{crit}} = 0.25$.

Case	u_i	h_i	ρ_i	Ri_i	x_m	ρ_m	u_m	h_m	Free-nose V_J	u_N	h_N	Drainage V_J	u_D	h_D
10	1.00	0.010	1050	0.005	1.70	1.02	0.27	0.105	0.098	0.223	0.142	0.059	0.178	0.184
11	0.50	0.010	1050	0.019	0.66	1.03	0.21	0.044	0.078	0.177	0.059	0.047	0.141	0.077
12	0.20	0.010	1050	0.117	0.13	1.04	0.16	0.015	0.058	0.130	0.020	0.034	0.103	0.026
13	0.50	0.020	1050	0.037	0.80	1.03	0.27	0.057	0.099	0.223	0.077	0.059	0.177	0.100

TABLE V. Examples for bottom GC and HM results for the same systems (cases) as in Table IV, dimensionless form. Lengths are scaled with h_i, and speed is scaled with $U = \sqrt{g_i' h_i}$ (given in the last column in m/s). $\Gamma = (\rho_m - \rho_i)/(\rho_i - \rho_a)$.

Case	u_i	$\frac{\rho_a}{\rho_i}$	Ri_i	x_m	$\frac{\rho_m}{\rho_i}$	u_m	h_m	Free-nose V_J	u_N	h_N	Drainage V_J	u_D	h_D	Γ	U
10	14.2	0.95	0.005	171	0.97	3.82	10.5	1.4	3.18	14.	0.84	2.5	18.	0.64	0.070
11	7.14	0.95	0.019	66	0.98	3.03	4.4	1.1	2.53	5.9	0.67	2.0	7.7	0.46	0.070
12	2.86	0.95	0.117	13	0.99	2.22	1.5	0.82	1.86	2.0	0.49	1.5	2.6	0.13	0.070
13	5.05	0.95	0.037	40	0.98	2.69	2.8	1.0	2.25	3.8	0.59	1.8	5.0	0.34	0.099

We use (7) unless stated otherwise. It is emphasized that the $\mathrm{Ri} = 1$ singularity detected in the steady-state formulation (6a)–(6c) does not appear in the time-dependent flow, and hence the same SW model can be applied for any value of $\mathrm{Ri}_{\mathrm{crit}}$. The Bq SW equations are recovered by setting $s = 0$ in (19b) and (21) [however, in (18) a small finite s is necessary for physical relevance].

The equations were solved by a finite-difference Lax-Wendroff method, with typically 500 grid points over the x domain and time step restricted by the Courant-Friedrichs-Lewy (CFL) condition (tests on different grids confirmed the reliability). The scheme has documented deficiencies of small spurious oscillations and dissipation [14] whose damping prevents sharp presentation of jumps, but the major behavior of the variables is well reproduced. Since the present investigation is focused on major effects [motion of the interface, formation and propagation of the internal jump, and change of regime (sub- vs supercritical)], the small numerical dissipation effects of the scheme are acceptable.

SW results and comparisons

Note that for E and c_D we use correlation (7) with $\mathrm{Ri}_{\mathrm{crit}} = 0.25$ unless stated otherwise.

We solved in detail case 2 of the top GC considered in Table I: In dimensional form mks units, $h_i = 0.2$, $u_i = 4.2$, $\rho_i = 0.6$, and $\rho_a = 1.2$. We obtain $g_i' = 4.9$, and the scaling speed is $U = 0.99$. This is a clear-cut non-Bq case, with $s = -0.50$. The development of the flow with time is shown in Figs. 6 and 7. Overall, the flow field is consistent with the predictions of the hybrid model. It is evident that a strong jump in h and u appears from the beginning. The jump is moving all the time. In the first stage, the height and length of the mixed region increase. In the second stage, the mixed region attains a fixed height h_m at x_m.

The effect of drainage is illustrated by the differences between Fig. 6 and Fig. 7. In Fig. 6 the GC propagates on an unbounded boundary. In Fig. 7 there is a free drainage edge at $x_D = 30$. The drainage begins at $t = 13.3$ when x_N of the free nose reaches the position x_D. Comparing the figures, we observe that the flow of the current in the domain $x < 30$ is very little influenced by the drainage condition. However, at $t = 35$ the internal jump is at $x_J = 27.6$, very close to the drainage point. The subsequent propagation of the jump is beyond the resolution of the thin-layer approximation. The jump is no longer needed, because after a short time interval the supercritical domain of the GC ($u = 3.2$) reaches the position $x_D = 30$ and can drain as a free jet. In other words, the internal jump is spilled out from the system at $t \approx 36$. The subsequent flow of the GC in the domain $0 < x < x_D = 30$ is expected to be a steady state without an internal jump. This is consistent with the prediction of the hybrid model.

Quantitatively, there is good agreement between the predictions of the HM and SW solution concerning the shape and velocities in the various domains. The SW and HM values of h_m, ρ_m, u_N, h_N, and V_J agree within about 2%. The disagreements can be attributed to the simplifications of the HM (constant height of the expanded domain) and numerical errors (dissipation) of the finite-difference solution (the jumps are not sharp). From the physical point of view, it is evident that the SW solution and the HM cover the same phenomenon. (However, a pointwise comparison of the time-dependent flow is problematic, because the HM begins with an established steady-state

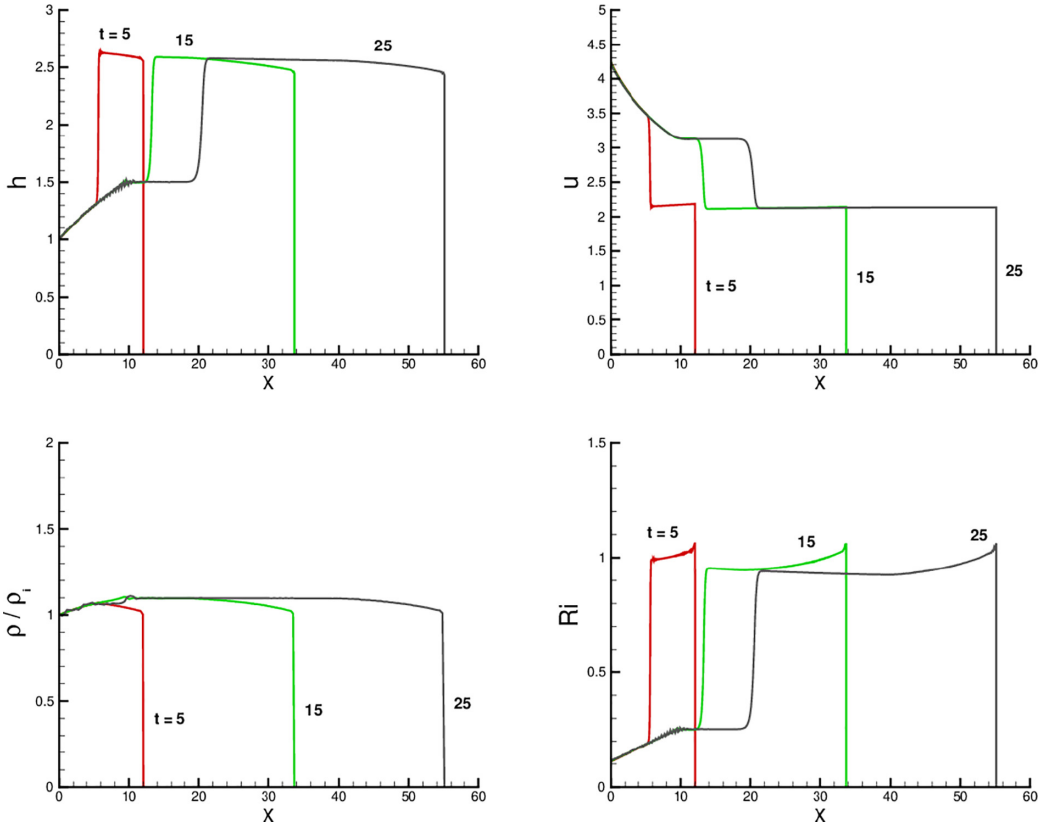

FIG. 6. SW results for case 2 at $t = 5, 15, 25$ with a free nose (no drainage). Top GC, h is measured downwards.

domain of length x_m.) The major conclusion for the system with $\mathrm{Ri}_{\mathrm{crit}} = 0.25$ is that the internal jump propagates with constant speed and leaves behind a domain of steady-state structure with constant h_m, ρ_m and supercritical speed u_m. This is a jetlike motion. We do not see any mechanism

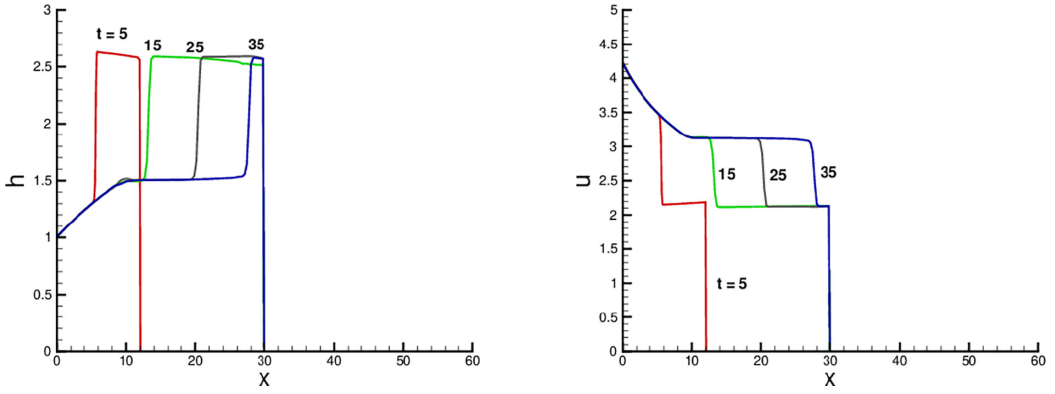

FIG. 7. SW results for case 2 at $t = 5, 15, 25, 35$ with a drainage at $x_D = 30$, $\mathrm{Ri}_{\mathrm{crit}} = 0.25$. Top GC, h is measured downwards.

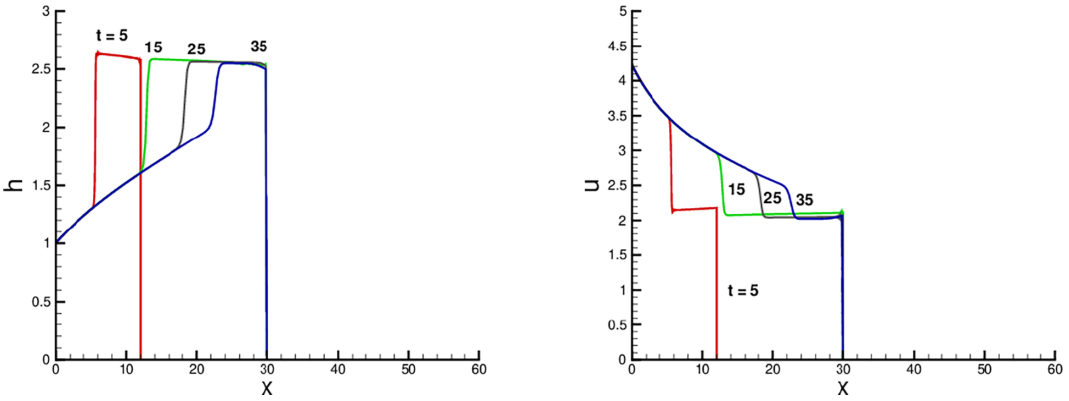

FIG. 8. SW results for case 2 at $t = 5, 15, 25, 35$ with a drainage at $x_D = 30$, $\mathrm{Ri}_{\mathrm{crit}} = 0.80$. Top GC, h is measured downwards.

that can stop the propagation of the jump and shrink back the jet. The scenario of a fixed internal jump, as considered by HVVV, does not apply to this system.

For the clarification of the effect of $\mathrm{Ri}_{\mathrm{crit}}$ on the flow, we changed the value $\mathrm{Ri}_{\mathrm{crit}} = 0.25$ used in Fig. 7 to $\mathrm{Ri}_{\mathrm{crit}} = 0.8$ in Fig. 8. This is the end-of-entrainment value reported in Ref. [3]. The drastic increase in $\mathrm{Ri}_{\mathrm{crit}}$ (by a factor of 3.2) causes a moderate quantitative change in the profiles of h and u (Figs. 7 and 8). The mixed domain (upward inclined h) becomes longer and higher, and speed u is more reduced. The value of maximum ρ/ρ_a (not shown) increases from 0.54 to 0.57 (the value at the source is 0.50). The qualitative structure is unchanged: The forward-moving internal jump is present, and the supercritical flow moves toward the drainage point. Again, we do not observe any tendency for arresting this jump and pushing it back to a fixed position as suggested by HVVV.

In a more drastic test, we changed $\mathrm{Ri}_{\mathrm{crit}} = 100$. Practically, this means that the effects of entrainment and drag are present all the time because in all our tests the values of Ri were below 3. In this framework we used three correlations: (i) Eq. (7), (ii) the formula of Ref. [15],

$$E = \frac{5.5 \times 10^{-3}}{a + \sqrt{a^2 + 0.15}}, \quad a = 3.6\mathrm{Ri} - 1; \quad c_D = 0.0065 \quad (\mathrm{Ri} \leqslant 100), \tag{22}$$

and (iii) a modification of the formula of Ref. [15], which has been used in the model of HVVV, namely,

$$E = \frac{5.5 \times 10^{-3}}{b + \sqrt{b^2 + 0.15}}, \quad b = 3.6\left(\frac{\rho}{\rho_a}\right)\mathrm{Ri} - 1; \quad c_D = 0.0065 \quad (\mathrm{Ri} \leqslant 100). \tag{23}$$

The SW results obtained with (22) are denoted as SWc. Note that c_D is the same in all correlations. The theoretical justification for the modification of (22) into (23) is not clear; the reason seems to be the empirical agreement with the simulations of HVVV. For a Bq system the difference between (22) and (23) is insignificant, but for a non-Bq top GC the latter formula predicts larger entrainment during the entire process.

Figure 9 shows a comparison of HVVV steady-state results with the present SW time-dependent solution (without drainage) at $t = t_1 = 18$ (the time when the free nose reaches the position $x_D = 40$). There is some agreement concerning the behavior of the density ρ in the current: an increase over a relatively short x_m and then a quite constant value over a long distance. Since $\rho_a/\rho_i = 2$, the mixing turns out to be small in all the shown results. The largest mixing is in the large-eddy simulated flow field. In the other variables (h, u, Ri) there are significant disagreements between the present and the HVVV predictions. The SW solution predicts a moving jump that leaves behind a fairly thin layer of high supercritical speed.

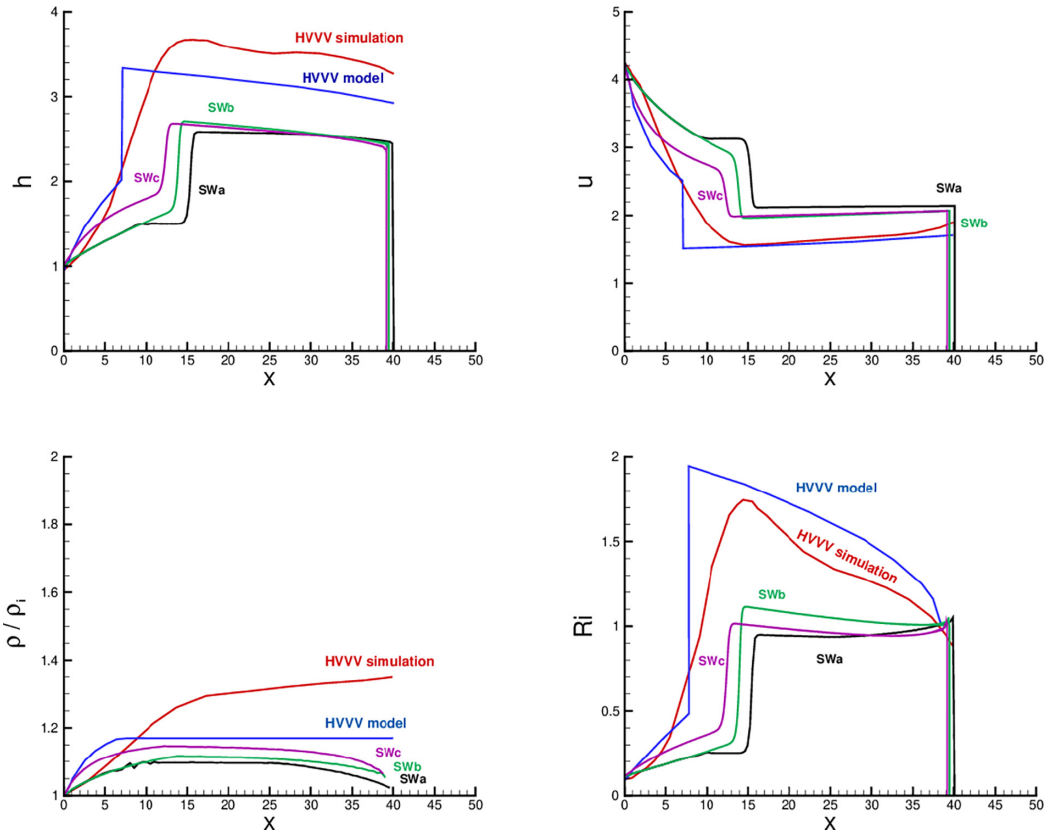

FIG. 9. Comparisons of HVVV steady-state simulation (red) and model (blue) case 2 with SW free nose at $t = 18$ for the following: SWa, correlation (7) with $\mathrm{Ri}_{\mathrm{crit}} = 0.25$; SWb, correlation (7) with $\mathrm{Ri}_{\mathrm{crit}} = 100$; and SWc, correlation (22). Top GC, h is measured downwards.

Consider the SWc solution, which uses the original [15] entrainment and drag correlations. At $t_1 = 18$ the SW free jump is at $x_J(t_1) = 12.5$, while the steady-state model of HVVV predicts $x_S = 7$. If such a steady state exists, a complex readjustment motion must occur, during which the jump is pushed back a significant distance. To check this hypothesis, we applied in the SW solution the critical condition $u_D = \sqrt{(g'h)_D}$ after the nose reaches x_D. The time-dependent solution is presented in Fig. 10. The profiles for $t = 25$ and 35 do not show a tendency of a backward-moving jump. However, the profiles show some oscillations that propagate from x_D upstream. Our interpretation is as follows. There are two possible scenarios. First, the oscillations generated at x_D prevail for a long time and preclude the reduction to a steady-state flow. Second, these oscillations will develop into a coherent forcing that will push back the jump to the theoretical steady-state x_S and reshape the flow in the subcritical domain. [Note that Eqs. (9) and (10) admit a negative V_J for a sufficiently large h^+/h_m. Since the height $h(x,t)$ in the subcritical domain $x_J(t) < x < x_D$ may increase after t_1, a backward internal jump is physically possible.] The reliable discrimination between these scenarios is beyond the resolution of our code. In any case, the adjustment process is expected to require a very long time, because the reflection effect is propagated by the backward-moving characteristics whose speed (dimensional) is $u - (g'h)^{1/2} = u(1 - \sqrt{\mathrm{Ri}})$, in the domain where Ri is close to 1. The presence of entrainment and drag complicates the analysis of these characteristics and precludes a simple analytical estimate of the reflection effect. A tentative (with low accuracy) SW solution with the present code, not shown in the figures, suggests that in case SWc the jump will be arrested at

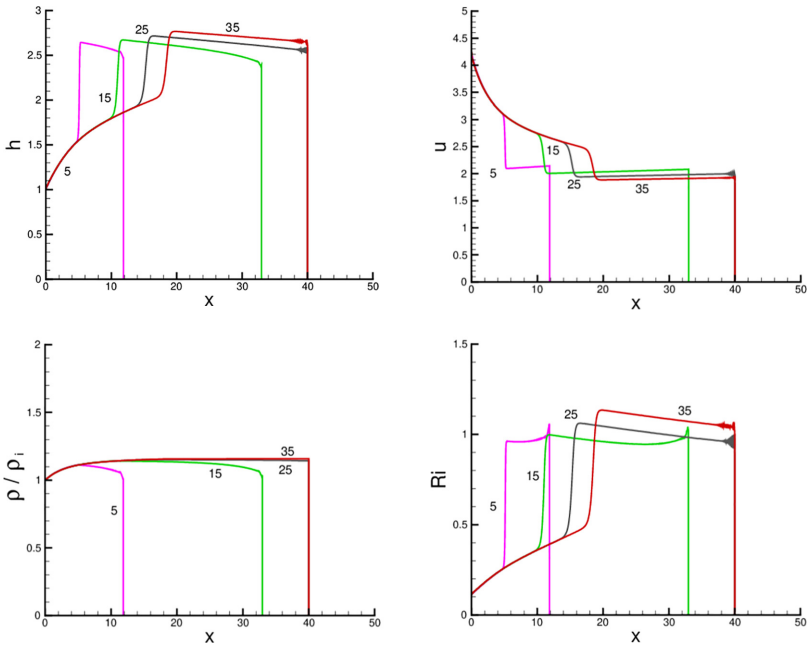

FIG. 10. SW results for free nose followed by critical u_D at $x_D = 40$, correlation (22). Top GC, h is measured downwards.

$t \approx 95$ at $x_J = 24.5$. Then it moves back slowly, with oscillations, such that $x_J \approx 23$ at $t = 200$. A more reliable long-time solution must be left for future investigation with more accurate codes. We also note that the time of reflection and adjustment to a tentative steady state is expected to increase with x_D. In the present examples, $x_D = 40$, but solutions for larger values of x_D (a practical possibility) will need results for even longer times than considered here.

Next, we performed the SW calculations using the modified correlation (23). The comparison with the simulation and model of HVVV is shown in Fig. 11. The propagation of the nose $x_N(t)$ is little affected by the change in the entrainment correlation; the nose reaches the edge slightly after $t_1 \approx 18$, and then a free drainage flow develops. The internal jump propagates quite fast initially, attaining $x_J = 10$ at $t = 18$. However, this propagation slows down during the drainage stage and stops at $x_J = 14$ at about $t = 50$. Subsequently, the internal jump clearly moves back, slowly, attaining $x_J = 12$ at $t = 100$. The profiles at $t = 100$ are in plausible agreement with the steady-state results of HVVV. The conclusion is that the SW solution with correlation (23) supports the possibility that the steady-state results of HVVV are a good approximation for the long-time behavior. However, it is still uncertain if and when the SW solution will reach a steady state; in Fig. 11 the jump overshoots x_S, is arrested, and then moves back. It is not clear if it will attain x_S and settle there. Our code is not sufficiently accurate for a reliable prediction of the flow for $t > 100$.

The initial conditions h_i, u_i, ρ_i and the value of x_D are also expected to affect the realization of a quasistationary jump at x_S (provided that $\mathrm{Ri}_{\mathrm{crit}} > 1$). A change in the initial conditions changes Ri_i; see (5). Supposing a fixed x_D (scaled with h_i), a decrease in Ri_i will increase x_S (scaled with h_i). (This can be inferred from the discussion in Sec. II B 2.) In this case, we expect that the arrested jump will need a shorter time for moving back to x_S, thus making the steady state a more plausible approximation. The opposite is expected when the change in the input conditions causes an increase in Ri_i. The effect of x_D is more obvious: For fixed initial conditions, an increase in x_D will decrease

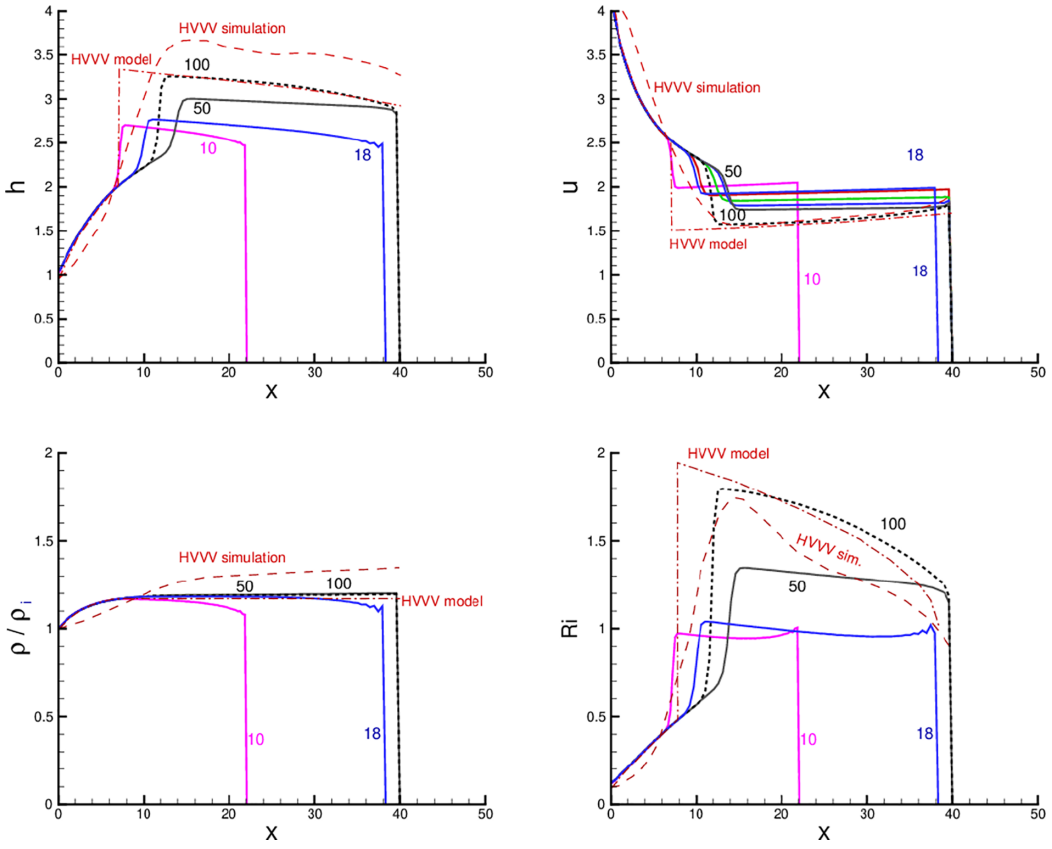

FIG. 11. SW results for free nose followed by critical u_D at $x_D = 40$, using correlation (23), and comparison with HVVV. The SW jump is arrested at $t = 50$ (solid black line), and the dashed black line shows the profile at $t = 100$. Top GC, h is measured downwards.

x_S (again, see Sec. II B 2). In this case, a longer time will be necessary for all the stages of the motion: arrival of the nose to x_D, arresting the jump, and also of the backward motion when relevant. The study of the details is left for future work.

The large-eddy simulations results of HVVV do not provide clear-cut support to the arrest of the internal jump and backward (or oscillatory) motion. The study is focused on the long-time solution and uses various averages of the flow field. The averages converge to some smooth quasisteady profiles, which seem to support the existence of a steady-state flow. We note that the averaged profiles of the large-eddy simulations do not show an internal jump; instead, they display a region of significant (but not sharp) variation of the variables roughly from x_S downstream over 5–10 units of h_i; see Figs. 9 and 11. This transition domain seems to agree with the distance of overshoot of the free jump in the time-dependent SW solutions. HVVV suggest that the nonsharp jump may be attributed to a local entrainment into the jump, but this does not contradict the possibility of a time-dependent flow in the transition domain.

The study in Ref. [3] does not support the steady-state flow with a stationary-jump hypothesis. The paper indicates that $E = 0$ for $\mathrm{Ri} > \mathrm{Ri}_{\mathrm{crit}} = 0.8$. This validates the HM solution, with no internal jump. One may argue that $E = 0$ does not necessarily impose $c_D = 0$, and this, theoretically, leaves open the possibility that Ri will increase toward the critical 1 according to (16). On the other hand, that study emphasizes that the flow was in (quasi)steady state only for a finite (short)

time period, after which a reflected bore from x_D upstream has been observed. This contradicts the long-time steady-state pattern of the HVVV model.

IV. CONCLUDING REMARKS

We considered the time-dependent process of a strongly supercritical ($\mathrm{Ri}_i = \mathcal{F}_i^{-2} < 0.25$) GC sustained by a source at $x = 0$. An open free drainage edge is present at $x_D \gg h_i$. Thus, eventually, a steady-state flow from $x = 0$ to x_D is expected. Using a hybrid model (HM) and finite-difference solution of the shallow-water (SW) equations, we demonstrated that the time-dependent flow is essential for the understanding of the steady-state solution.

The initial adjustment of the GC is as follows. The nose $x_N(t)$ propagates with a fairly constant u_N toward x_D. An internal jump appears at $x_J(t)$ with speed $V_J < u_N$. In the $x < x_J$ domain the flow is supercritical, with a significant quasisteady entrainment region in which ρ_i is mixed toward ρ_a, h increases, and u decreases. In the $x > x_J$ domain the expanded flow is subcritical, with constant or slightly-increasing-with-x velocity u. At some time t_1 the nose reaches the drainage edge, and the readjustment of the subcritical domain occurs; this, however, does not affect much the propagation of the internal jump for a significant time. When $\mathrm{Ri}_{\mathrm{crit}} < 1$, the internal jump will reach the drainage point x_D at t_2; this leaves behind, in $0 \leqslant x \leqslant x_D$, a steady-state supercritical flow with a smooth interface (no internal jump).

When $\mathrm{Ri}_{\mathrm{crit}}$ is large, the flow for $t > t_1$ is ambiguous. Theoretically, as shown by HVVV, a steady state with a stationary internal jump at $x_S < x_D$ is possible. The SW time-dependent calculations show that $x_J(t_1) > x_S$ (the overshoot is significant). The time-dependent process that may push back the jump to x_S is expected to be long and is beyond the accuracy of our solver. After t_1 (when the nose overflows x_D), some disturbances propagate upstream from the edge x_D; we detected some oscillations, and even the tendency of arresting, and pushing back, the internal jump. It is not clear if the long-time flow will tend to a steady state or not. The answer must be left for future work using more sophisticated codes. In any case, our study demonstrates that the behavior of E, c_D as functions of Ri is essential in the long-time flow.

The large-eddy numerical simulation results of HVVV cover only the averaged long-time ($t \gg t_1$) behavior of the system. The simulations show global agreement with the concept of an internal jump at a fixed position but do not really confirm the presence of the jump (the corresponding changes are smeared over a significant distance). The mechanism that places the internal jump (or its smeared counterpart) at the final position is not clear. We note in passing that the reproduction of a free-edge drainage at the outflux boundary in a numerical Navier-Stokes simulation is a challenge (see Refs. [11,16]). HVVV do not elaborate on this issue. The details of this boundary condition, and the difference with the weir boundary condition, may turn out to be significant for the presence or absence of a steady-state flow at large times. Again, these topics require further investigation that must be left for future work.

In typical cases, the speed of the current during free propagation and during drainage is fairly well reproduced by the classical results $cB_0^{1/3}$, where B_0 is the buoyancy flux (unaffected by entrainment) and c is a coefficient of magnitude 1.1–1.3.

The investigation is relevant to bottom and top GCs, in Boussinesq (Bq) and non-Bq systems. The differences are quantitative and typically not significant. However, we note that the definition of $\mathrm{Ri} = g'h/u^2$ may be ambiguous, because the reference density in g' may be either ρ of the current or ρ_a of the ambient. We use the former option but keep in mind that the values of $\mathrm{Ri}_{\mathrm{crit}}$ and the entrainment correlations of a Bq system may need recalibration when applied to non-Bq cases.

We considered a one-layer model. Extensions to two-layer models, taking into account the motion of the ambient along the lines of Ref. [8] are feasible, but not straightforward; see Ref. [1], Sec. 27.1.

This study demonstrates the importance of the time-dependent behavior of the flow and the availability of effective tools for the analysis of such flows. We argue that the studies based on steady-state formulations are an oversimplification that should be used with care, and perhaps

only as a supplement to a time-dependent analysis. In general, it is not clear if and when a steady-state flow appears for given boundary conditions, and in some cases the transient stage may be significantly different from the steady state for a long time period. Moreover, a steady-state GC is relevant only to a constant-source supply, and this is a serious restriction in practice.

The insights gained in this paper may provide an alternative interpretation to the observations of Ref. [3]. The GC in the experiment (Fig. 1 in that paper) displayed a steady flow for a few seconds; then, at t_w a strong upstream wave propagated from the edge x_D toward the source. We speculate that the short steady state was actually the flow before the internal jump reached the edge, i.e., $x_J(t_w) = x_D$. We keep in mind that in the experiment there was a weir at x_D, not a true open edge. We speculate that t_w corresponds to t_2 of our models: At t_w the supercritical current hit the weir. This strong impact is bound to produce a significant reflected bore into the upstream direction.

Our analysis highlights the importance of a possible $\mathrm{Ri}_{\mathrm{crit}} < 1$ above which entrainment and drag are negligible. The available information is inconclusive. Most E and c_D data were obtained indirectly, using Bq GCs over inclined boundaries. For example, HVVV employ a correlation, derived in 1996 from experiments with a Bq fluid mud over a sloping bottom, to model non-Bq GCs of hot air below a flat ceiling; the Reynolds numbers are different, and even the definition of the relevant Richardson number is debatable. We argue that in these circumstances, no clear-cut conclusions concerning the horizontal supercritical GC can be stated with confidence. Careful experiments (laboratory and computer simulations) dedicated to this problem are necessary, and we are confident that the present study will provide useful guidelines and data for comparison for these future works.

ACKNOWLEDGMENT

Thanks are extended to Prof. A. J. Hogg for useful discussions on the topic and to an anonymous referee for improvement suggestions.

APPENDIX: BASIC SW BALANCES

We use dimensional variables. For definiteness, during the formulation we consider a bottom ("heavy") GC. The implementation to the top ("light") current is explained after (A10). The bottom is at $z = 0$, and the gravity is in the $-z$ direction. The interface between the current and the ambient is $z = h(x, t)$, and the height-averaged velocity of the GC is $u(x, t)$. The ambient is stationary. The density ρ of the current and the dimensionless dilution fraction α are functions of x and t.

The density of the current is expressed by

$$\rho = \rho_c = \rho_a + (\rho_i - \rho_a)\alpha, \tag{A1}$$

where $\alpha \in [0, 1]$ ($\alpha = 1$ means undiluted, and $\alpha = 0$ means fully diluted).

The volume continuity is given by

$$\frac{\partial h}{\partial t} + \frac{\partial uh}{\partial x} = E|u|. \tag{A2}$$

The right-hand-side term expresses the rate of volume entrainment through the interface. This is a normal velocity, and hence consistency with the SW assumptions imposes the restriction $E \ll 1$ which is in general satisfied.

For mass continuity, we note that the entrainment carries fluid of density ρ_a, which is mixed with the local ρ. This yields

$$\frac{\partial \rho h}{\partial t} + \frac{\partial \rho uh}{\partial x} = E|u|\rho_a. \tag{A3}$$

Combining with (A2) (multiplied with ρ_a), we obtain

$$\frac{\partial(\rho-\rho_a)h}{\partial t}+\frac{\partial(\rho-\rho_a)uh}{\partial x}=0. \tag{A4}$$

This equation shows that the density excess (i.e., the buoyancy) is conserved in the GC. The balance (A4) can be rewritten as

$$\frac{\partial \alpha h}{\partial t}+\frac{\partial \alpha uh}{\partial x}=0 \tag{A5}$$

or

$$\frac{\partial g'_e h}{\partial t}+\frac{\partial g'_e uh}{\partial x}=0, \tag{A6}$$

where $g'_e=\alpha g'_i$ is the effective reduced gravity.

For the momentum equation, we first employ the hydrostatic equation and the condition of pressure continuity at the interface. In the stationary ambient the (reduced) pressure is a constant, set here to 0. Let $\Delta\rho=(\rho-\rho_a)$. We obtain the pressure in the current

$$p=g\Delta\rho(h-z)\quad(0\leqslant z\leqslant h), \tag{A7}$$

and hence

$$\frac{\partial p}{\partial x}=g\left[(h-z)\frac{\partial\Delta\rho}{\partial x}+\Delta\rho\frac{\partial h}{\partial x}\right]\quad(0\leqslant z\leqslant h). \tag{A8}$$

The driving pressure for the current is therefore

$$-\int_0^h\frac{\partial p}{\partial x}dz=-\frac{1}{2}g\frac{\partial\Delta\rho h^2}{\partial x}. \tag{A9}$$

The x-momentum equation expresses the balance between the inertial, pressure gradient, and drag over the layer of thickness h as follows:

$$\frac{\partial\rho uh}{\partial t}+\frac{\partial\rho u^2h}{\partial x}=-\frac{1}{2}\frac{g|\Delta\rho|h^2}{\partial x}-c_D\rho|u|u. \tag{A10}$$

Note that $g|\Delta\rho|=\rho_a g'_e$. (In the bottom GC the change of $\Delta\rho$ to $|\Delta\rho|$ is trivial because $\rho>\rho_a$.)

The volume and mass balances are kinematic relationships, and hence (A2)–(A6) apply directly to the top GC. The analysis of the dynamic effect of the buoyancy requires some care, and the conclusion is that the change of $\Delta\rho$ to $|\Delta\rho|$ in the momentum equation (A10) and in the definitions of the reduced gravity g' render the present formulation valid for both bottom and top GCs.

Standard mathematical manipulation of (A1)–(A6) and (A10) yields various convenient forms of the equations of motion. In particular, for the steady state we obtain (6a)–(6c).

The system of equations is hyperbolic and admits discontinuities (jumps). The jump conditions can be obtained by a control volume analysis [1]. Since the jump is over a very small Δx, the local density is not influenced by the entrainment $\sim E\Delta x/h$, and hence the classical results remain a good approximation (taking care to use the local density). In particular, we have the following: (1) For the free-nose jump we can use

$$u_N=\mathrm{Fr}_N(g'_ih_N)^{1/2}=\mathrm{Fr}_N[|1-\rho(x_N)/\rho_a|gh_N]^{1/2}, \tag{A11}$$

where Fr_N is Benjamin's Froude formula. The non-Bq effect is incorporated in the value of g'_i. (2) For the internal jump, we use (9) and (10).

The reduction $E = c_D = 0$

When entrainment and drag are negligible, the SW formulation is significantly simplified by setting $E = c_D = 0$ in the balance equations. In this case, $\rho = \rho_c = \rho_i = \text{const}$; hence $g'_e = \text{const}$, and $\alpha = 1$. The equation for α can be discarded. The governing equations are

$$\frac{\partial h}{\partial t} + \frac{\partial uh}{\partial x} = 0, \tag{A12}$$

$$\frac{\partial uh}{\partial t} + \frac{\partial}{\partial x}\left[\rho u^2 h + \frac{1}{2} g'_i h^2\right] = 0. \tag{A13}$$

These equations are evidently satisfied by a sustained flow with piecewise-constant h and u, separated by an internal jump at $x_J(t)$ and ending with a free-nose jump of height h_N at $x_N(t)$, as discussed in Sec. II A.

[1] M. Ungarish, *Gravity Currents and Intrusions: Analysis and Prediction* (World Scientific, Singapore, 2020).

[2] C. G. Johnson and A. J. Hogg, Entraining gravity currents, J. Fluid Mech. **731**, 477 (2013).

[3] T. H. Ellison and J. S. Turner, Turbulent entrainment in stratified flows, J. Fluid Mech. **6**, 423 (1959).

[4] S. Haddad, S. Vaux, K. Varrall, and O. Vauquelin, Theoretical model of continuous inertial gravity currents including a jump condition, Phys. Rev. Fluids **7**, 084802 (2022).

[5] M. E. Negretti, J.-B. Flor, and E. J. Hopfinger, Development of gravity currents on rapidly changing slopes, J. Fluid Mech. **833**, 70 (2017).

[6] P. Odier, J. Chen, and R. E. Ecke, Entrainment and mixing in a laboratory model of oceanic overflow, J. Fluid Mech. **746**, 498 (2014).

[7] J. S. Salinas, M. I. Cantero, M. Shringarpure, J. Fedele, D. Hoyal, and S. Balachandar, Slope dependence of self-similar structure and entrainment in gravity currents, J. Fluid Mech. **934**, R4 (2022).

[8] A. Hogg, M. M. Nasr-Azadani, M. Ungarish, and E. Meiburg, Sustained gravity currents in a channel, J. Fluid Mech. **798**, 853 (2016).

[9] M. Shringarpure, H. Lee, M. Ungarish, and S. Balachandar, Front condition of high-Re gravity currents produced by constant and time-dependent influx: an analytical and numerical study, Eur. J. Mech. B: Fluids **41**, 109 (2013).

[10] Q. Guo, Y. Z. Li, H. Ingason, Z. Yan, and H. Zhu, Theoretical studies on buoyancy-driven ceiling jets of tunnel fires with natural ventilation, Fire Saf. J. **119**, 103228 (2021).

[11] M. Momen, Z. Zheng, E. Bou-Zeid, and H. A. Stone, Inertial gravity currents produced by fluid drainage from an edge, J. Fluid Mech. **827**, 640 (2017).

[12] M. Ungarish, C. G. Johnson, and A. J. Hogg, A novel hybrid model for the motion of sustained axisymmetric gravity currents and intrusions, Eur. J. Mech. B: Fluids **49**, 108 (2015).

[13] M. Ungarish, C. G. Johnson, and A. J. Hogg, Sustained axisymmetric intrusions in a rotating system, Eur. J. Mech. B: Fluids **56**, 110 (2016).

[14] K. W. Morton and D. F. Mayers, *Numerical Solutions of Partial Differential Equations* (Cambridge University Press, Cambridge, 1994).

[15] T. van Kessel and C. Kranenbureg, Gravity current of fluid mud on sloping bed, J. Hydraul. Eng. **122**, 710 (1996).

[16] M. Ungarish, L. Zhu, and H. A. Stone, Inertial gravity current produced by the drainage of a cylindrical reservoir from an outer or inner edge, J. Fluid Mech. **874**, 185 (2019).